CRACK GROWTH PATH AND SIF DISTRIBUTION STUDIES IN 3D CASES

C. W. SMITH
Department of Engineering Science and Mechanics
Virginia Polytechnic Institute and State University
Blacksburg, Virginia 24061-0219

ABSTRACT

Using a refined frozen stress method, the author and his colleagues have studied the growth, shapes and stress intensity factor (SIF) distributions for real cracks in a number of practical engineering problem geometries over the past twenty years. After briefly outlining the method, the present paper utilizes results selected from these studies to formulate general concepts governing the behavior of such cracks during stable growth. A brief review of the algorithms associated with the method is included in the Appendix.

KEYWORDS

Three dimensional cracks, stress intensity factor, frozen stress photoelasticity, crack growth.

INTRODUCTION

Although most fracture problems involve three dimensional (3D) aspects, they are often small enough to ignore. In other cases, however, 3D effects may appear to be significant, and the present intent is to examine cases common to engineering practice where 3D effects are apparent and an attempt to form some general observations from measurements in such problems.

Beginning some 20 years ago, the author (Smith, 1975) and his colleagues began to study ways for measuring crack shapes, growth and stress intensity factor (SIF) distributions in some fairly simple problems involving 3D effects.

Method of Analysis

The method of analysis selected was frozen stress photoelasticity, applied with certain refinements to bodies containing real cracks (Smith and Kobayashi, 1993). The procedure followed involved the following steps:

i) We focus on surface cracks since, in most service failures, cracks begin at the surface of the body. By striking a sharp blade held normal to the body, a planar, semi-elliptic crack will emanate a short distance into the body and arrest.

ii) After heating the model above critical temperature and loading, the starter crack is grown to its desired size. The crack shape is determined by the loads and body shape and is generally not known a-priori.

iii) Once the crack reaches desired size, the load is reduced to stop crack growth and the remaining stress is "frozen in."

iv) Thin slices are then removed mutually orthogonal to the flaw border and its local surface for analyses at points along the flaw border.

v) In order to increase the number of fringes for accuracy, the Post (Post, 1966) and Tardy (Tardy, 1929) methods are applied in tandem during the slice analysis by the polariscope.

vi) The optical slice data are fed into an algorithm for converting the optical data into SIF estimates for each slice. The Mode I algorithm is given in the Appendix. Since the present discussion is confined to stably growing cracks, only the Mode I algorithm is needed, since such growth always occurs under pure Mode I loading at the crack tip.

SELECTED EXPERIMENTS

In selecting experimental results to focus our general observations on, it was decided to use those from only one type of loading (internal pressure), and only on growing cracks which are believed to simulate fatigue crack growth paths under pure Mode I loading in isotropic, homogeneous media.

Motor Grain Geometries

Long, cylindrical bodies with central perforations of various shapes such as shown in Fig. 1 are typical of rocket motor grain. In Fig. 1, the centerline of each fin is an axis (or plane) of symmetry (S) and any crack initiating at a fin tip (P) in a plane of symmetry will remain in that plane as it grows. However, the semi-elliptic crack will change its aspect ratio (a/c) (Fig. 1) as it grows in order to reduce or eliminate the SIF gradient along the flaw boder.

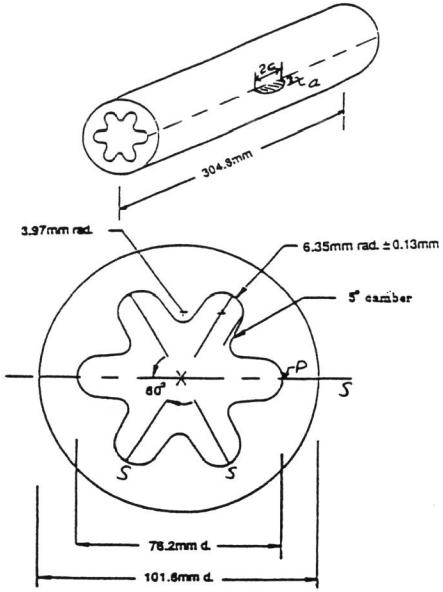

Fig. 1 Motor Grain Model Dimensions

A typical SIF distribution for such a crack is virtually uniform. By keeping the cracks near the mid-length of the cylinder, they remain symmetric with respect to the minor axis (depth direction a) of the crack as well. If a fin tip starter crack is slightly tilted to the plane of symmetry, it will grow back into the plane of symmetry as it grows under pressure. In the event a crack initiates away from the fin tip, its subsequent growth pattern under internal pressure creates a non-planar crack (Fig. 2). In order to follow this crack growth, we focus on the crack path of the mid-point of the crack border. The crack surface remains symmetric with respect to this path, and to compute normalized SIF factors, we introduce the concepts of a' and ϕ' (see Appendix). As shown in Fig. 2, when the initial crack is pressurized above critical temperature, it first changes direction or kinks,and then grows along a smooth path. The kink results from the fact that the initial crack is usually not in a principal plane produced by the internal pressure. Subsequent to kinking, the crack mid-point appears to follow closely the principal surface produced by the internal pressure loading of an uncracked model. The extent to which this is true is shown in Fig. 3.

In Fig. 3, the path of the mid-point of the real crack is compared with the principal direction in an uncracked model obtained both photoelastically and from a two dimensional finite element model. The SIF distribution for such cracks is typically non-uniform (Fig. 4). Further details of the study leading to the above observations are found in Smith, *et al.*, (1993).

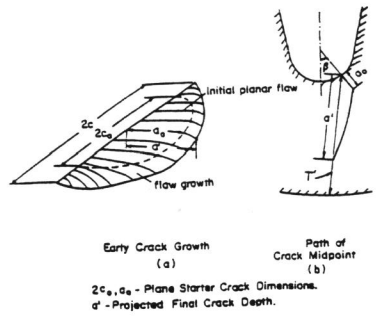

Fig. 2 Growth of crack not initiated in plane of symmetry

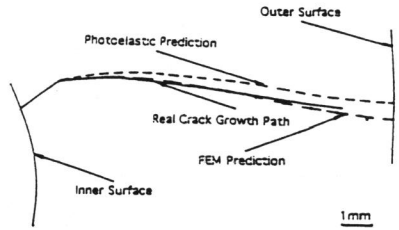

Fig. 3 Path of midpoint of crack initated off the plane of symmetry determined three ways

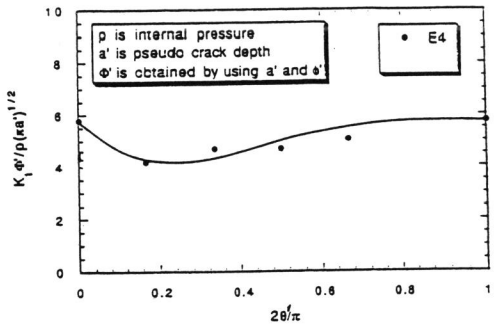

Fig. 4 SIF Distribution for crack emanating from the location $\beta = 45°$ (For Φ', a', θ', see Appendix)

Pressure Vessel Nozzle Geometries

A second common problem geometry which leads to three dimensional crack problems occurs when cracks emanate from the juncture of a pressure vessel with a nozzle. A photo of the photoelastic model of a boiling water reactor is shown in Fig. 5 with nozzle corner notation in Fig. 6. In this study, three initial crack orientations were considered as shown in Fig. 7. These cracks were initially nearly quarter-elliptic rather than semi-elliptic due to the nozzle geometry. The 0° location flaw was in the principal plane of the vessel and remained there as it grew under pressure with increasing aspect ratio a_v/a_n (Fig. 6). The SIF distribution became more uniform as the crack grew (Fig. 8).

Stable Growth Path Anomalies

Although the present study was confined to stably growing cracks, there were encountered circumstances during which a sharp change in crack surface orientation resulted in a rapid

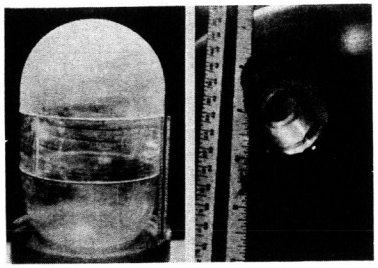

Fig. 5 Photo of reactor vessel with nozzle model

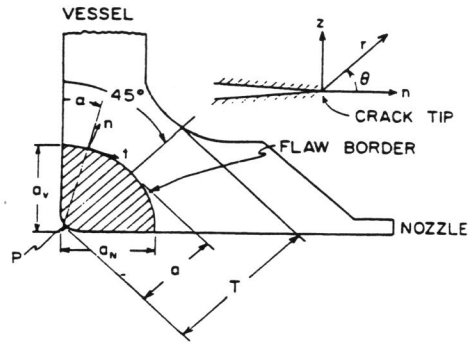

Fig. 6 Nozzle corner notation

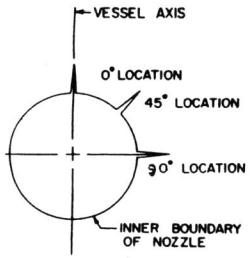

Fig. 7 Initial crack orientations

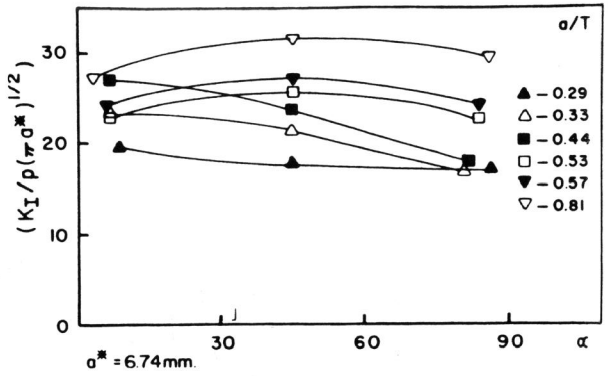

Fig. 8 Normalized SIF distributions $\theta = 0°$

redistribution of the SIF distribution along the crack front. We refer to these changes as stable growth path anomalies and note several cases below.

The 90° location flaws were initially in a principal plane of the nozzle which was 90° from the maximum principal plane in the vessel. These cracks also remained planar as they grew with increasing aspect ratio a_v/a_n. However, slight tilting of the starter crack out of the principal plane would cause the crack to turn rather sharply towards the principal plane ($\theta = 0°$) in the vessel wall. Moreover, the SIF distribution in these cracks became more non-uniform with increasing crack depth (Fig. 9). Because of their tendency to turn away from a principal plane when given slight initial misorientation, the $\theta = 90°$ crack path was considered to exhibit an anomalie due to problem geometry.

By far the most interesting of the nozzle corner cracks were the 45° location cracks (Fig. 10). Initially, these cracks, like the others, were planar quarter-elliptic cracks. However, when

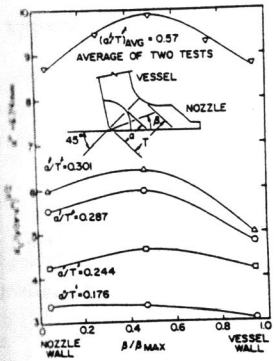

Fig. 9 Normalized SIF distributions $\theta = 90°$

they were caused to grow by internal pressure above critical temperature, the part of the crack front near the nozzle wall (n) extended in its plane while the part of the crack front near the vessel wall (m) kinked into a new path and proceeded along a curved path. There appeared to be a region near P where the planar part of the crack near the nozzle intersected the curved surface of the part of the crack influenced by the vessel wall. During the early part of the crack growth, the maximum normalized SIF occurred near this juncture. Then, between $a/T = 0.291$ and 0.458, the discontinuity at P disappeared and a radical redistribution of the SIF resulted Fig.(11) with a smooth non-planar crack surface and a maximum SIF at the vessel wall.

This behavior suggests a competing role between the nozzle and vessel wall effects which produced a crease in the crack surface joining the two surfaces until, at a certain depth (between $a/T = 0.291$ and 0.458) the vessel wall effect smoothed the crease out of the crack surface, eliminating the point of discontinuity at P. Details of this study are found in Smith, *et al.*, (1979)

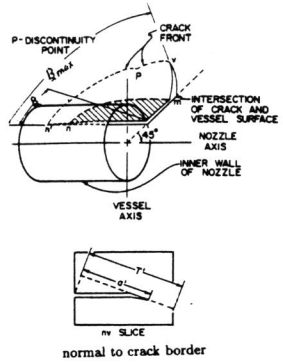

Fig. 10 Initial and grown crack fronts $\theta = 45°$ with associated notation

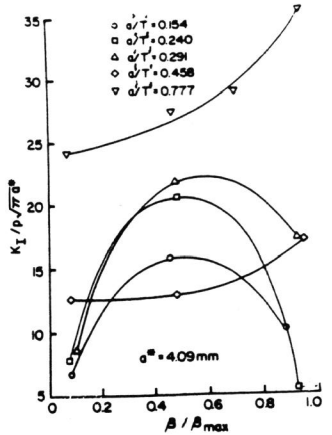

Fig. 11 SIF distributions for $\theta = 45°$ cracks

A somewhat similar effect was observed when starter cracks initiated off the fin axis in the motor grain models kinked. The SIF distribution which, for the semi-elliptic starter crack was a maximum at maximum depth changed radically during turning of the crack but became more uniform again after being fully turned. The center of the crack turned first, reducing the SIF there and increasing it near the turned part closest to the part of the crack yet to turn (Fig. 12), that is, a shift in the region of highest SIF occurred until the crack was completely turned. Then the SIF distribution returned to a more conventional form with the maximum SIF at or near the center of the fully turned crack and stable growth continued.

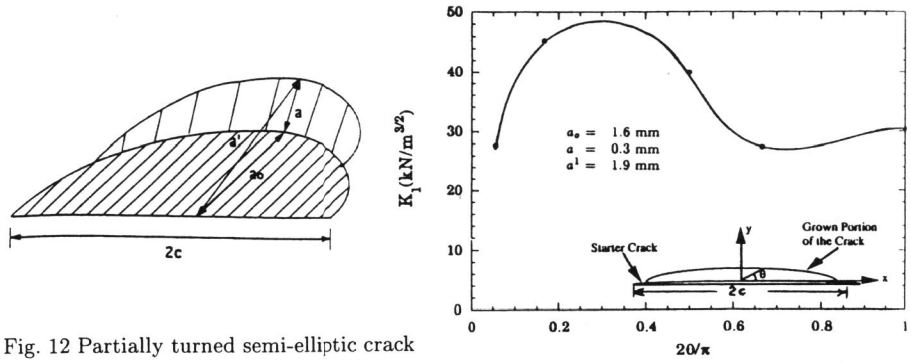

Fig. 12 Partially turned semi-elliptic crack

GENERAL OBSERVATIONS

Based upon the foregoing observations (and others) it appears that stably growing cracks exhibit pure Mode I loading. For such cases:

i) If a starter crack develops in a plane of symmetry, it will remain in that plane as it grows. As it grows, its aspect ratio changes to minimize the SIF gradient along the crack front.

ii) If a starter crack is near to, but not in a plane of symmetry, it will move to that plane under Mode I loading.

iii) Starter cracks not located near planes of symmetry will migrate to a nearby principal surface of stress and continue growth in that surface.

iv) When cracks kink or change their surface orientations rather suddenly, SIF redistribution along the flaw border is likely to occur. This appears to be related to the shedding of a shear mode near the crack tip in contrast to gentle curving of a crack surface due to remote effects.

v) In all cases studied in stable crack growth, the crack path is conjectured to follow closely a principal surface in the uncracked model due to the applied load.

The present discussion has focused on a very limited class of practical fracture problems. However, the extent of applicability of the above observation is believed to be quite general for stable crack growth in isotropic, homogeneous media.

ACKNOWLEDGMENTS

The author wishes to acknowledge the support of the staff and facilities of the Virginia Tech Department of Engineering Science and Mechanics and the following program directors and their agencies for parts of the above study: Dr. Clifford Astill, National Science Foundation; Mr. Gene Maddux, Wright-Patterson AFB; Dr. J.C. Newman, Jr. and Mr. C.C. Pue, NASA Langley Research Center; and especially, Mr. John Merkle, Oak Ridge National Laboratory; Dr. C.T. Liu, Phillips Laboratory; and former students, Dr. A. Wang, Dr. W. Peters, Dr. M. Jolles, Dr. A. Andonian, T.S. Fleishman, and W.T. Hardrath.

APPENDIX A

Mode I Algorithm For Determination of Stress Intensity Factor (SIF)

In linear elastic fracture mechanics (LEFM) using the photoelastic approach, one can begin with Mode I near-tip equations (Fig. A.1)

$$\sigma_{ij} = \frac{K_I}{\sqrt{8\pi r}} f_{ij}(\theta) + \sigma^o_{ij}(i,j = n,z) \qquad (A-1)$$

where K_I is the Mode I SIF, σ^o_{ij} are the contribution of the nonsingular stresses in the measurement zone, and r, θ then centered at the crack tip. The following expression is computed for the maximum shear stress $\tau^{nz}_{\max}$, in truncated form, along $\theta = \pi/2$, the direction of fringe spreading under Mode I loading (Fig. A.2).

$$\tau^{nz}_{\max} = \frac{K_{Ap}}{\sqrt{8\pi r}} = \frac{K_I}{\sqrt{8\pi r}} + \tau_o \qquad (A-2)$$

where K_{Ap} is an "apparent" SIF which includes the effects of σ^o_{ij} $\left\{\text{i.e., } \tau_o = f\left(\sigma^o_{ij}\right)\right\}$ with the singular effect in the measurement zone. The stress-optic law states that $\tau^{nz}_{\max} = \frac{Nf}{2t}$ where N is the measured stress fringe order, f is the material fringe value and t the slice thickness. Thus $\tau^{nz}_{\max}$ is proportional to N and may be regarded as the measured quantity together with r. By rearranging terms in Eq. A-2 and normalizing, we can obtain

$$\frac{K_{Ap}\Phi}{p\sqrt{\pi a}} = \frac{K_I\Phi}{p\sqrt{\pi a}} + \frac{\sqrt{8}}{p}\tau_o\Phi\left(\sqrt{\frac{r}{a}}\right) \qquad (A-3)$$

for a semi-elliptic crack where the coefficient of $\sqrt{r/a}$ is a constant, p is the internal pressure and a is the crack size. Φ is an elliptic integral which varies with the aspect ratio of the crack (a/c). Its form is given in Fig. A-3 where Φ is just a normalizing factor.

Equation A-3 suggests that the normalized K_{Ap} varies linearly with the square root of the normalized distance from the crack tip $\left\{\sqrt{r/a}\right\}$ in the singularity dominated zone.

Thus, by plotting the digitized raw data, $\left[K_{Ap}\Phi/p\sqrt{\pi a}\right]$ versus $\left[\sqrt{r/a}\right]$, the linear zone may be found. Then using a least squares fit, the line representing these data can be constructed and extrapolated across a near-tip nonlinear zone to determine the normalized K_I [i.e., $K_I\Phi/p\sqrt{\pi a}$] at the crack tip. The linear zone is normally just outside $\sqrt{r/a} \approx 0.2$, but should be at the same location for all slices on the same crack. Fig. A-3 illustrates this process for an interior slice from the flaw border.

Non-planar cracks emanating from semi-elliptic starter cracks are studied by replacing a by a' (Fig. 2) and Φ by Φ' (Fig. A-3) in the above equations provided the cracks are turned over their entire length, with θ' in the plane of a' and $2c$.

For the nozzle corner cracks, a more direct form of Eq. A-3 can be written as:

$$\frac{K_{AP}}{p\sqrt{\pi a}} = \frac{K_1}{p\sqrt{\pi a}} + \frac{\sqrt{8}}{p}\tau_o\sqrt{\frac{\pi}{a}} \qquad (A-4)$$

A general discussion of the method including all three modes of analysis is found in (Smith, 1993).

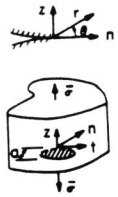

Fig. A-1 Problem Geometry and local notation for Mode I

Fig. A-2 Mode I fringe pattern prior to Post and Tardy refinement

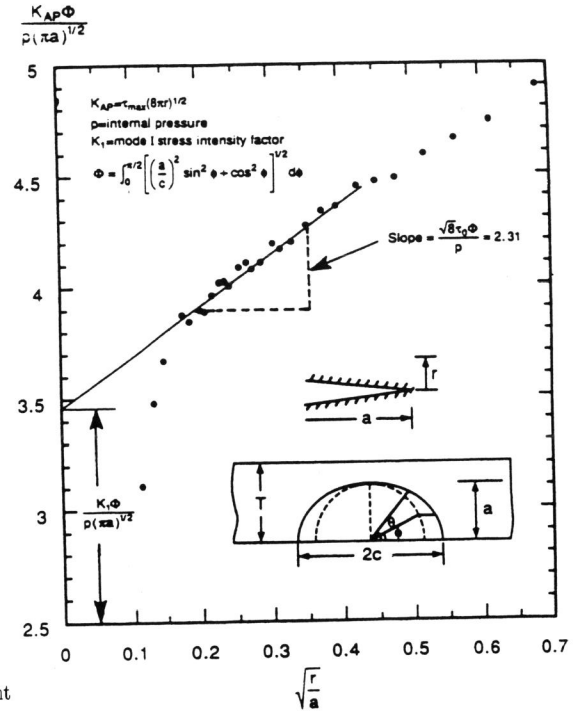

Fig. A-3 Determination of K_1 from slice data

REFERENCES

Smith, C.W. (1975). Use of three dimensional photoelasticity and progress in related areas. *Experimental Techniques in Fracture Mechanics 2*, Society for Experimental Stress Analysis, Chap. 1, 3–58, Iowa State University Press, Ames, Iowa and Society for Experimental Stress Analysis, Westport, Connecticut.

Smith, C.W., Peters, W.H., Hardrath, W.T., and Fleishman, T.S. (1979). Stress intensity distributions in nozzledcracks of complex geometry. Paper No. G4/4, *Transactions of the 5th Int. Cont. on Structural Mechanics in Reactor Technology*, **G**, 8pp.

Smith, C.W. (1993). Experimental determination of stress intensity distributions in engineering problems. *Applied Mechanics Reviews*, Vol. 46, No. 11, Pt. 2, 529–540.

Smith, C.W., Wang, A.L., and Liu, C.T. (1993). Experimental determination of crack growth and SIF determination in motor grain models. *Novel Experimental Techniques in Fracture Mechanics*, ASME-AND Vol. 76, 101–112.

Smith, C.W. and Kobayashi, A.S. (1993). Experimental fracture mechanics. In: *Handbook on Experimental Mechanics*, 2nd Rev. Ed. (Kobayashi, A.S., ed.), Chap. 20, 905–968.

Post, D. (1966). Fringe multiplication in three dimensional photoelasticity, *J. Strain Analysis*, Vol. 1, No. 5, 380–388.

Tardy, M.L.N. (1929). Methode pratique d'examen de mesure de la birefringence des verres d'optique, *Opt. Rev.*, Vol. 8, 59–69.